Raman spectroscopy studies of Ce-doping effects on $Ba_{0.5}Sr_{0.5}TiO_3$ thin films

S. Y. Wang, B. L. Cheng,[a] Can Wang, S. Y. Dai, K. J. Jin, Y. L. Zhou, H. B. Lu, Z. H. Chen, and G. Z. Yang
Beijing National Laboratory for Condensed Matter Physics, Institute of Physics, Chinese Academy of Sciences, Beijing 100080, China

(Received 21 March 2005; accepted 14 November 2005; published online 4 January 2006)

$Ba_{0.5}Sr_{0.5}TiO_3$ (BST) thin films are among the best-known ferroelectric and dielectric materials. Ce-doped BST films have been fabricated by pulsed laser deposition in order to enhance their dielectric properties. X-ray diffraction, atomic force microscopy, and Raman spectroscopy have been used to study variations of crystal structure, surface morphologies, and phase stability of Ce-doped BST films, respectively. A strong influence of Ce doping on the properties of the BST films has been observed. First, a small amount of Ce dopant makes easy epitaxial growth of a BST film with a smooth surface on a MgO substrate. Second, residual stress in a BST film on a MgO substrate can be reduced by Ce doping, as demonstrated by the blueshift of phonon peaks in Raman spectroscopy. © *2006 American Institute of Physics*. [DOI: 10.1063/1.2150263]

I. INTRODUCTION

In the last decade, barium strontium titanate $[Ba_{1-x}Sr_xTiO_3$ (BST)] thin films have attracted great attention because of their favorable performance in tunable microwave device applications, in fast nonlinear optics applications, and in high-density-gigabit dynamic random access memory applications.[1,2] The physical properties of BST films are strongly influenced by the composition,[3] dopant,[4,5] deposition conditions,[6] internal stress,[7,8] and electronic structure,[9] etc. BST is an insulator at room temperature due to its large band-gap value. However, controlled doping can change its physical properties, such as electronic structures, core levels, and dielectric properties. For instance, dopants of Nb or Sb, substituted at the Ti site, result in *n*-type electrical properties in $SrTiO_3$ film.[10,11] Higuchi *et al.* reported the electronic structure of a *p*-type $SrTiO_3$ single crystal in which Sc^{3+} was introduced into the Ti^{4+} site as the acceptor ion.[12] Guo *et al.*[13] reported the structural phase transitions in $SrNb_xTi_{1-x}O_3$ ($x=0.0-0.5$) films. Dai *et al.*[5] studied the electronic structure of $SrIn_{0.1}Ti_{0.9}O_3$ *p*-type film. The addition of a small amount of aliovalent ions ($<5\%$) exhibits a different influence on the physical properties of a BST film. Kim and Park reported that doping of 0.5 at. % Al decreased the leakage current of BST film, and the same amount of Mn doping decreased it further; however, the same amount of Nb doping greatly increased the leakage current.[14] Cole *et al.* investigated the effects of Mn impurities on BST film using x-ray photoemission spectroscopy, and proposed that Mn acted as an electron acceptor compensating for the charge density in nominally undoped films.[15] Rare-earth elements Ce-doped BST have been investigated and shown strong influence on the dielectric and optical properties of BST. Yu *et al.* found that a Ce dopant made the dielectric characteristics of the bulk $BaCe_xTi_{1-x}O_3$ solid solutions more diffuse and dispersed.[16] The ferroelectric and stress behaviors of the bulk Ce-doped $BaTiO_3$ solid solutions were investigated by Ang *et al.*; they found high strain level of 0.14%–0.19% with a small hysteresis under 60 kV/cm in Ce-doped $BaTiO_3$.[17] Liu *et al.* found that the Ce-doped $BaTiO_3$ thin films showed a larger linear electric-optic coefficient and obvious hysteresis in the quadratic electro-optic coefficient.[18] In our recent work, we found that Ce doping can decrease the leakage current in the BST thin film; furthermore, the Ce-doped BST deposited on a MgO substrate exhibited lower surface roughness than that of an undoped BST film.

Raman spectroscopy has been used as a nonperturbing probe for thin-film characterization. It is well known that Raman spectroscopy is a characterization method to measure the frequencies of the long-wavelength lattice vibrations (phonons). Unlike x-ray diffraction (XRD), which provides a direct determination of the crystal structure, Raman spectroscopy can give useful information on impurity, grain size, porosity, and crystal symmetry. Furthermore, Raman scattering is greatly influenced by disorder and residual stress: these can cause variation in phonon frequencies and lifetime, leading to the broadening of Raman peaks. Therefore, Raman spectroscopy has been demonstrated as a powerful tool to study stress and size effects in ferroelectric thin films. The lattice dynamics and Raman spectra of bulk materials, $BaTiO_3$ (Refs. 19–21) and $SrTiO_3$,[22] have been investigated in detail. Raman studies on the BST thin films, whose lattice-dynamical properties are influenced by the stress and defects in the films, have also been reported.[23–26]

In this paper, investigation with Raman spectroscopy on the stress of acceptor Ce-doped BST films is presented. Undoped BST film prepared under the same conditions is also investigated as compared.

II. EXPERIMENTAL PROCEDURE

The undoped 1.0 and 5.0 at.% Ce-doped $Ba_{0.5}Sr_{0.5}TiO_3$ (CeBST) films are grown by pulsed laser deposition tech-

[a]Author to whom correspondence should be addressed; electronic mail: blcheng@aphy.iphy.ac.cn

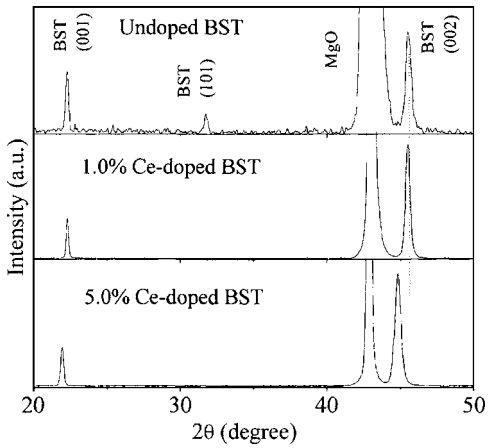

FIG. 1. X-ray-diffraction pattern of undoped and Ce-doped $Ba_{0.5}Sr_{0.5}TiO_3$ thin films deposited on MgO substrates.

nique employing a XeCl excimer laser (308 nm, 20 ns, and 4 Hz). The detailed information on the fabrication of ceramic targets and films have been described elsewhere.[3] The thickness of CeBST films is measured to be about 200 nm by a surface profile measuring system (DEKTAK III, U. S. A.). The crystalline phase and structure of the CeBST films are analyzed by XRD employing Cu $K\alpha$ radiation (40 kV, 50 mA) and a graphite monochromator. The surface morphologies of the CeBST films are observed with Nano Scope III atomic force microscopy (AFM). Raman measurements for CeBST samples are performed at room temperature in the backscattering geometry with a Jobin-Yvon T64000 triple Raman spectrometer. A 488 nm Ar^+ laser line of 100 mW is used for excitation. The incident light and the scattering light are perpendicular to the sample surface. The spectrometer provides a wave-number resolution of ~ 0.5 cm^{-1} and accuracy of ~ 0.1 cm^{-1}. All measurements are performed at room temperature.

III. XRD AND AFM RESULTS

The CeBST films grown on MgO substrates possess a perovskite structure, and have preferred orientation along the (001) direction due to the (001) MgO substrate, as shown in Fig. 1. The crystal phase along the (101) direction can also be observed in undoped BST film; however, it disappears in Ce-doped BST films. That means that the undoped BST thin films are deposited with polycrystalline structure on MgO, but the Ce-doped BST films are grown epitaxially along the (001) direction, normal to the MgO substrate surface. Such phenomenon can be ascribed to the increase of lattice constant due to Ce doping. The lattice parameter (c) along the vertical-substrate direction of the CeBST film increases from 3.991 to 4.002 Å (1% CeBST) and 4.039 Å (5% CeBST), calculated from the average of the peak position of (001) and (002) in Fig. 1. The lattice parameter (a) along the parallel-substrate direction of the CeBST film increases from 3.966 to 3.982 Å (1% CeBST) and 4.028 Å (5% CeBST), calculated from the measured position of peaks (101) and (303) in XRD Φ scan and θ-2θ scan. The ratio of c/a is 1.006, 1.005, and 1.003 for undoped BST, 1% CeBST, and 5% CeBST, respectively. Therefore, the lattice parameters c and a increase with Ce concentration, while the ratio of c/a decreases. Obviously, the tetragonality of CeBST thin films decreases with an increase of Ce content. The increased lattice parameter with Ce concentration indicates that Ce ions have dissolved into the BST lattice. X-ray photoelectron spectroscopy measurement confirmed that Ce ions in the CeBST thin film are only trivalent.[27] Because the ionic radii of Ce ions (Ce^{3+} = 1.01 Å) are larger than that of Ti^{4+} (0.61 Å), but smaller than that of Ba^{2+} (1.35 Å) or Sr^{2+} (1.18 Å), the increased lattice parameter implies that Ce ions substitute onto the B site of the ABO_3-type perovskite, BST. It is well known that a random, polycrystalline film contains more grain boundary than an epitaxial film does, and the grain boundaries are often the sites for charge segregation and subsequent charge decay, deteriorating the dielectric and electric properties. Therefore, Ce doping may be helpful to increase the dielectric and electric properties of a BST film on a MgO substrate.

The surface morphologies of undoped and Ce-doped BST films are shown in Figs. 2(a)–2(c): the surface roughness becomes more and more smooth with increasing Ce concentration in BST films. The root-mean-square surface roughness (R_{rms}) of the films, determined via tapping model AFM, decreases from 25 nm in the undoped BST film to 7.0 and 4.8 nm in 1.0 and 5.0 at. % Ce-doped BST films, respectively. Such results originate from the increase of lattice constant of the CeBST films, because the larger lattice of the CeBST films is more compatible with the lattice of the MgO substrate (a=4.213 Å), which cause relatively smoother surface of the CeBST.

IV. RAMAN SPECTRUM AND DISCUSSION

A. Raman spectrum results

In order to compare the paraelectric (cubic) and ferroelectric (tetragonal) features in Raman spectra at room temperature, the Raman spectra of $Ba_{0.5}Sr_{0.5}TiO_3$ (BST-0.5) and $Ba_{0.7}Sr_{0.3}TiO_3$ (BST-0.3) ceramics have been measured, as shown in Figs. 3(a) and 3(b); for the cubic BST-0.5 ceramic, there are only two broad bands centered at 226 and 576 cm^{-1} for the Raman spectrum. In bulk BST-0.3 ceramic, all remarkable features of tetragonal structure can be clearly found, including a broad peak centered at 226 cm^{-1}, a weak shoulder peak at 303 cm^{-1}, an asymmetric peak near 515 cm^{-1}, and a broad, weak peak at 730 cm^{-1}, which are very similar to the results reported previously, as summarized in Table I,[21] except for a slight shift of peaks position. Both in the paraelectric and ferroelectric phases, the ABO_3 perovskite has one molecule (five atoms) per unit cell and twelve long wavelength optical modes. The paraelectric phase has cubic (O_h^1 or $Pm3m$) symmetry. The optical modes in this phase transform according to the triply degenerate irreducible representations of the O_h point group: $\Gamma_{cub} = 3F_{1u} + F_{2u}$. The F_{1u} modes are infrared active, and the F_{2u} is the so-called "silent mode" since it is neither infrared nor Raman active, and so there is no Raman activity in the paraelectric phase with perfect cubic symmetry. In the ferroelectric phase with tetragonal (C_{4v}^1 or $p4mm$) symmetry, each triply degenerate F_{1u} mode splits into a doubly degenerate E mode and a nondegenerate A_1 mode, while the F_{2u} silent

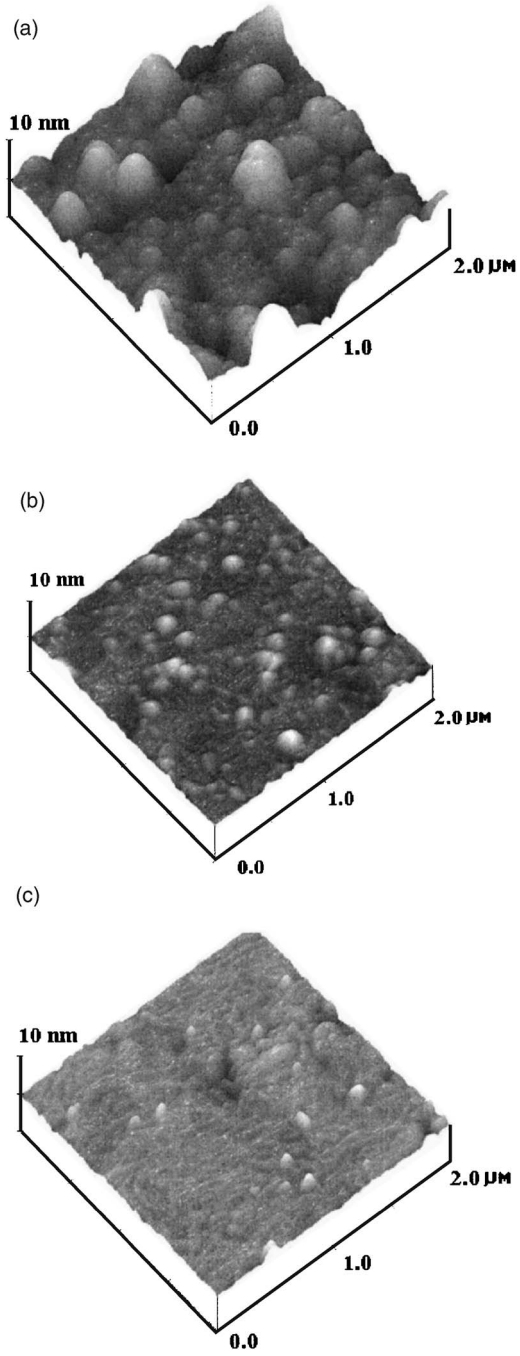

FIG. 2. AFM image of undoped and Ce-doped $Ba_{0.5}Sr_{0.5}TiO_3$ thin films for different Ce concentrations: (a) undoped BST, (b) 1.0 at. % Ce, and (c) 5.0 at. % Ce. (X:0.5 μm/div: Y:5 nm/div).

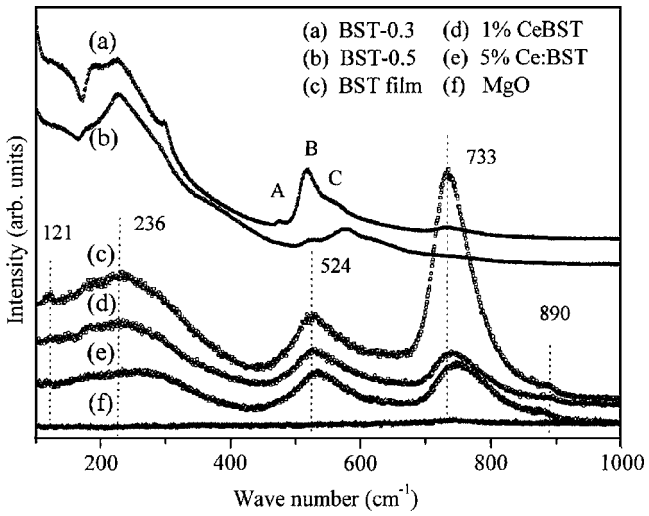

FIG. 3. Room-temperature Raman spectra of (a) ceramic BST-0.3, (b) ceramic BST-0.5, (c) undoped BST film, (d) 1% CeBST film, (e) 5% CeBST film, and MgO substrate.

mode splits into B_1 and E modes. Thus, $\Gamma_{tet}=3A_1+4E+B_1$. All the A_1 and E modes are infrared and Raman active, while the B_1 mode is only Raman active. The presence of a long-range electrostatic force further splits each of the A_1 and E modes into transverse-optical (TO) and longitudinal-optical (LO) components. A compilation of the optical phonon frequencies and their symmetry in tetragonal $BaTiO_3$ have been summarized by Venkateswaran *et al.* as shown in Table I.[21] The peaks at 303 and 730 cm^{-1}, which are specific to the tetragonal phase of BST, appear in BST-0.3 but not in BST-0.5 spectrum, confirming that at room temperature the BST-0.3 and BST-0.5 are at ferroelectric (tetragonal) and paraelectric (cubic) phases, respectively. There is a dip near 168 cm^{-1} in the two Raman spectra of BST-0.3 and BST-0.5 ceramics, which has been understood as an interference due to unharmonic coupling between the three A_1(TO) phonons.[24]

Raman spectra of undoped, Ce-doped BST films, and MgO substrate are shown in Fig. 3, MgO substrate shown as curve (f), with no Raman activity in the frequency range from 100 to 1000 cm^{-1}. The dominant features in three CeBST curves are a broad peak centered at 236 cm^{-1} [A_1(TO)], an asymmetric and broad peak around 524 cm^{-1} [A_1,E(TO)], and a broad strong peak at around 733 cm^{-1} [A_1,E(LO)], where the phonon assignment is given inside square brackets. The observed Raman peaks have been assigned to more than one phonon mode since the frequencies of a few A_1 and E modes are very close (see Table I), and the different orientation of the crystallites in a polycrystalline sample does not allow polarization selection between the A_1 and E modes. As Ce concentration increases, the A_1(TO) phonon peaks at 236 and 524 cm^{-1}, and the A_1(LO) phonon peak at 733 cm^{-1} shifts to a high wave number (blueshift). Furthermore, the LO phonon at 733 cm^{-1} becomes progressively weak and broad. The optical phonon frequencies (ω) and their mode symmetry assignments in undoped and Ce-doped BST thin films are summarized in Table II. As mentioned earlier, the peak at 733 cm^{-1} is spe-

TABLE I. Optical phonon frequencies (ω) and their mode symmetry assignments in tetragonal $BaTiO_3$ (Ref. 21).

ω (cm^{-1})	Symmetry	ω (cm^{-1})	Symmetry
170	A_1(TO)	475	A_1(LO)
185	E(TO+LO)	486	E(TO)
270	A_1(LO)	518	E(TO)
305	A_1(TO)	520	A_1(TO)
305	E(TO+LO)	715	E(TO)
463	B_1	720	A_1(LO)

TABLE II. Comparison of the shift of various phonon modes (cm^{-1}) in BST-0.5 ceramics and pulsed-laser-deposited undoped and Ce-doped BST thin films.

	disorder activated	A_1 (TO1)	A_1 (TO2)	A_1 (LO3)	Stress At interface
BST-0.5 ceramic	···	226	578	···	···
Undoped BST	122	236	524	733	890
1% CeBST	···	240	526	736	888
5% CeBST	···	269	534	749	872

cific to the tetragonal phase of BST. Thus, Raman spectra confirm that our CeBST thin films on the MgO substrate are tetragonal in structure although the single crystal or ceramic with the same composition is a cubic one. The intensity of the A_1(LO) mode is much higher in the undoped BST film than in Ce-doped BST films, which probably originates from the polycrystalline structure and larger tetragonality in undoped BST film. In Fig. 3, two weak peaks are observed at about 121 and 890 cm^{-1}. The low-frequency peak (121 cm^{-1}) seen only in undoped BST film probably caused by disorder-activated scattering from the acoustic TA and LA phonon branches, which have a high density of states at the Brillouin zone boundary, as proposed by Yuzyuk *et al.*[25] The weak peak (~890 cm^{-1}) which existed in undoped and Ce-doped BST films probably originated from the residual stress at the interface between the thin film and the MgO substrate.[13]

B. Residual stress analysis

The observed blueshifts of Raman peaks A_1(TO1) mode centered at 236 cm^{-1}, the A_1(TO2) at 524 cm^{-1}, and A_1(LO3) at 733 cm^{-1}, as shown in Fig. 4, are attributed to the change of residual stress due to Ce doping.[6,21] As mentioned above, Ce ion at the *B*-cation site is considerably heavier than Ti ion, which tends to decrease the vibration frequencies, as reported by Dixit *et al.*[28] in Zr-doped $BaZr_xTi_{1-x}O_3$ thin films, that a downshift in the mode frequency was observed with the increase of Zr doping. Such change is not observed in this work probably due to a major effect of residual stress which tends to result in an upshift in the mode frequency. For $PbTiO_3$ thin films, Raman frequencies shift remarkably to lower frequency compared with a single crystal, and such shifts can be well accounted for by compressive stress.[29] In our case of CeBST thin films as well as those observed by Chen *et al.*[6] and Zhu *et al.*,[7] Raman modes centered at A_1(TO1), A_1(TO2), and A_1(LO3) are found at higher frequencies than the corresponding modes in a single crystal. Now, we try to analyze the origin the residual stress in BST thin films, and compare the present Raman data with the hydrostatic pressure effect on $BaTiO_3$ and $PbTiO_3$ bulks in order to understand the blueshift of the A_1 modes.

Stress in the BST thin film can be caused by lattice parameter and thermal expansion mismatch between film and substrate, the volume expansion associated with compositional deficiencies such as Ba, Sr, and O vacancies, as shown in Fig. 5. The stress due to the lattice mismatch $x_l=(a_s-a_f)/a_f$, and thermal expansion mismatch $x_l=(\alpha_s-\alpha_f)\Delta T$ are considered to be major parts in the stress formation in thin films. In the stress expressions of x_l and x_t a_s (4.213 Å) and a_f(3.960 Å) are the equilibrium lattice parameters of substrate and film, respectively, and α_s ($13.8\times10^{-6}/°C$) and α_f($10.5\times10^{-6}/°C$) the thermal expansion coefficients of the substrate and film, respectively.[30] For BST thin films on MgO, the lattice of the film may be expanded near the interface to match to the larger lattice of the substrate and consequently tensile stress may remain in the BST thin film. In the process of cooling from the deposition temperature, BST thin films are compressive due to thermal coefficients mismatch on cooling. Furthermore, the oxygen vacancies also result in the volume expansion of the lattice, inducing the stress in the BST film. Therefore, there are three competing forces affecting the stress field of the film, which generate film stress. It is proposed by Chang *et al.*[31] that although most of the stress is relieved by the formation of misfit dislocations, residual stress still exist in the BST films.

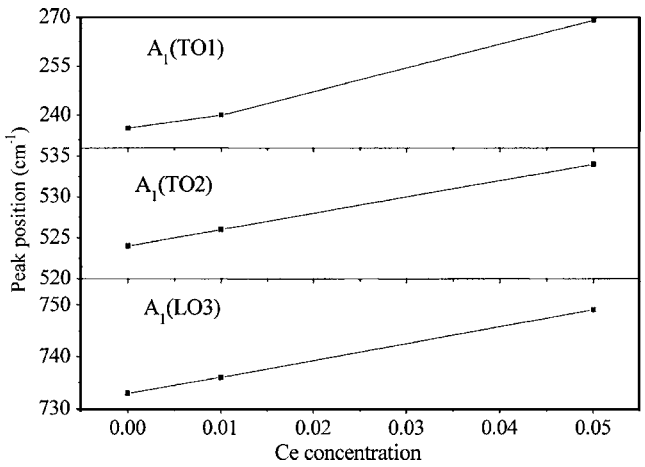

FIG. 4. Frequency of the Raman modes observed in undoped and Ce-doped BST thin films plotted as a function of Ce concentration.

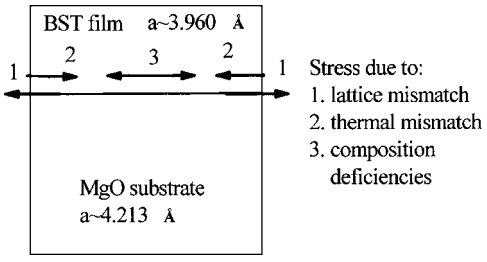

FIG. 5. Schematic diagram of possible force factors affecting the stress field of BST thin film on MgO substrate.

The total residual stress can be decomposed into hydrostatic and biaxial components using the elastic compliance tensor.[8] The hydrostatic component (U_{hyd}) can affect all three axes of the unit cell identically, while the biaxial component (U_{bi}) can affect the two in-plane axes (a and b) directly and the out-of-plane axis (c) indirectly by means of Poisson's ratio. Such decomposition of stress helps in understanding the effect of each stress component because the potential sources of hydrostatic stress (interstitials, oxygen vacancies, etc.) are physically different from those of biaxial stress (substrate interactions, etc.).

C. Analysis on blueshifts of Raman modes

All lattice parameters of CeBST films are larger than that of the bulk lattice constant of the BST-0.5 target, indicating that the films have a growth-induced, positive hydrostatic stress probably due to interstitials, oxygen vacancies, and/or other defects. Because the larger Ce (ion radii Ce^{3+} = 1.01 Å) ions are substituted into the Ti (Ti^{4+}=0.61 Å) site of perovskite BST, as the Ce concentration is increased, the positive hydrostatic stress grows stronger in Ce-doped BST thin film. Venkateswaran *et al.* studied the Raman-scattering spectra of polycrystalline $BaTiO_3$ under hydrostatic pressure, and they proposed that within the stable region of the tetragonal phase of $BaTiO_3$ below 2 GPa, Raman peaks of the A_1(TO1) mode (at 270 cm^{-1}) shift to lower frequencies with increasing negative hydrostatic pressure.[21] At the same time, such positive hydrostatic pressure can also induce a blueshift of the A_1(LO3) mode (at 720 cm^{-1}), due to the larger c-axis lattice parameter.[6] Therefore, the Ce dopant induced by the positive hydrostatic pressure could be responsible for the shift of Raman models of A_1(TO1) and (LO3), which are plotted as a function of Ce-doping concentration in Fig. 4. Meanwhile, however, Venkateswaran *et al.*[21] observed that the E(TO) and A_1(TO) modes (in the range of 500–600 cm^{-1}) do not show any significant pressure-induced frequency shift, but there is a significant change in the line shape. Such change of line shape is similar to the results observed in our bulk BST-0.3 and BST-0.5 Raman spectra, as shown in Fig. 3. With increasing Sr concentration in bulk BST, Raman peaks labeled A, B, and C show obvious shift to higher frequency and the change of peak intensity. Such phenomenon accompanies the change of crystal structure of perovskite from the tetragonal phase to the cubic one. The blueshift of the A_1(TO2) mode at 520 cm^{-1} can be ascribed to the change of the crystal structure of CeBST films, as revealed by XRD that the Ce doping induces a decrease of tetragonality of the CeBST thin film. The increasing lattice parameter of CeBST films reduces the lattice mismatch between the MgO substrate and CeBST films, which eventually decrease the residual tensile biaxial stress in the CeBST films. Such phenomenon has also been demonstrated by the increase of surface smoothness of CeBST films, for large stress can result in a rough film surface. In Ce-doped BST films, the relative small biaxial stress decreases the tetragonality of the BST thin film. It can be seen from Fig. 3 that the peaks in cubic BST-0.5 exhibit a shift to higher frequencies compared with tetragonal BST-0.3 ceramic. Therefore, the smaller biaxial stress in Ce-doped BST films results in the blueshift of A_1(TO2) modes and the decrease of intensity and broad peak of the A_1 Raman peak.

V. SUMMARY

We have deposited undoped and Ce-doped BST films on a MgO substrate and investigated the influence of Ce doping on the crystal structure, surface morphologies, and residual stress of the BST thin film. The Ce doping results in the expansion of the lattice of the BST film due to the large atomic radii of the dopant of Ce. Such expansion makes the lattice of the BST film more compatible with that of the MgO substrate, and subsequently reduces the residual stress and surface roughness of the BST film. Raman peaks of the A_1(TO1) mode centered at 236 cm^{-1}, the A_1(TO2) at 524 cm^{-1}, and A_1(LO3) at 733 cm^{-1} are shifted to higher wave numbers with increasing Ce concentration. The good morphology, structure, and stress state of the Ce-doped BST film, compared to the undoped BST film, suggest that Ce doping is an effective way to optimize the BST film to be used in tunable microwave devices.

ACKNOWLEDGMENTS

The work is supported by the "Hundreds Talents Project" of the Chinese Academy of Sciences and the National Natural Science Foundation of China.

[1] K. J. Choi *et al.*, Science **306**, 1005 (2004).
[2] N. K. Pervez, P. J. Hansen, and R. A. York, Appl. Phys. Lett. **85**, 4451 (2004).
[3] S. Y. Wang, B. L. Cheng, C. Wang, W. Peng, H. B. Lu, Y. L. Zhou, Z. H Chen, and G. Z. Yang, Key Eng. Mater. **280–283**, 18 (2005).
[4] S. Y. Wang, B. L. Cheng, C. Wang, S. Y. Dai, H. B. Lu, Y. L. Zhou, Z. H Chen, and G. Z. Yang, Appl. Phys. Lett. **84**, 4116 (2004).
[5] S. Y. Dai, H. B. Lu, F. Chen, Z. H. Chen, Z. Y. Ren, and D. H. L. Ng, Appl. Phys. Lett. **80**, 3545 (2002).
[6] M. S. Chen, Z. X. Shen, S. H. Tang, W. S. Shi, D. F. Cui, and Z. H. Chen, J. Phys.: Condens. Matter **12**, 7013 (2000).
[7] J. S. Zhu *et al.*, J. Appl. Phys. **81**, 1392 (1996).
[8] C. M. Carlson, P. A. Parilla, T. V. Rivkin, J. D. Perkins, and D. S. Giniey, Appl. Phys. Lett. **77**, 3278 (2000).
[9] V. Cracium and R. K. Singh, Appl. Phys. Lett. **76**, 1932 (2000).
[10] T. Zhao, H. B. Lu, F. Chen, S. Y. Dai, G. Z, Yang, and Z. H. Chen, J. Cryst. Growth **212**, 451 (2000).
[11] H. H. Wang *et al.*, Appl. Phys. Lett. **78**, 1676 (2001).
[12] T. Higuchi, T. Tsukamoto, N. Sata, M. Ishigame, Y. Tezuka, and S. Shin, Phys. Rev. B **57**, 6978 (1998).
[13] H. Z. Guo, L. F. Liu, Y. Y. Fei, W. F. Xiang, H. B. Lu, S. Y. Dai, Y. L. Zhou, and Z. H. Chen, J. Appl. Phys. **96**, 3404 (2003).
[14] S. S. Kim and C. Park, Appl. Phys. Lett. **75**, 2554 (1999).
[15] M. W. Cole, P. C. Joshi, and M. H. Ervin, J. Appl. Phys. **89**, 6336 (2001).
[16] Z. Yu, C. Ang, Z. Jing, P. M. Vilarinho, and J. L. Baptista, J. Phys.: Condens. Matter **9**, 3081 (1997).
[17] C. Ang, Z. Yu, Z. Jing, R. Y. Guo, A. S. Bhalla, and L. E. Cross, Appl. Phys. Lett. **80**, 3424 (2002).
[18] Y. W. Liu, Z. H. Chen, C. L. Li, D. F. Cui, Y. L. Zhou, G. Z. Yang, and Y. Zhu, J. Appl. Phys. **81**, 6328 (1997).
[19] C. H. Perry and D. B. Hall, Phys. Rev. Lett. **15**, 700 (1965).
[20] M. DiDomenico, Jr., S. H. Wemple, and S. P. S. Porto, Phys. Rev. **174**, 522 (1968); M. Didomenico, Jr., S. H. Wemple, and S. P. S. Porto, Phys. Rev. Lett. **19**, 855 (1967).
[21] U. D. Venkateswaran, V. M. Naik, and R. Naik, Phys. Rev. B **58**, 14256 (1998).
[22] P. A. Fleury and J. M. Worlock, Phys. Rev. **174**, 613 (1968).
[23] D. A. Tenne, A. Soukiassian, X. X. Xi, H. Choosuwan, R. Guo, and A. S.

Bhalla, J. Appl. Phys. **96**, 6597 (2004).
[24]Y. I. Yuzyuk, V. A. Alyoshin, I. N. Zakharchenko, E. V. Sviridov, A. Almeida, and M. R. Chaves, Phys. Rev. B **65**, 134107 (2002).
[25]Y. I. Yuzyuk, J. L. Sauvajol, P. Simon, V. L. Lorman, V. A. Alyoshin, I. N. Zakharchenko, and E. V. Sviridov, J. Appl. Phys. **93**, 9930 (2003).
[26]D. A. Tenne, A. Soukiassian, M. H. Zhu, A. M. Clark, X. X. Xi, H. Choosuwan, Q. He, R. Guo, and A. S. Bhella, Phys. Rev. B **67**, 012302 (2003).
[27]S. Y. Wang *et al.*, J. Phys. D **38**, 2253 (2005).
[28]A. Dixit, S. B. Majumder, A. Savvinov, R. S. Katiyar, R. Guo, and A. S. Bhalla, Mater. Lett. **56**, 933 (2002).
[29]J. A. Sanjurjo, E. L. Cruz, and G. Burns, Phys. Rev. B **28**, 7260 (1983).
[30]W. Chang, J. S. Horwitz, A. C. Carter, J. M. Pond, S. W. Kirchoefer, C. M. Gilmore, and D. B. Chrisey, Appl. Phys. Lett. **74**, 1033 (1999).
[31]W. Chang, C. M. Gilmore, W. J. Kim, J. M. Pond, S. W. Kirchoefer, S. B. Qadri, D. B. Chirsey, and J. S. Horwitz, J. Appl. Phys. **87**, 3044 (2000).